Graphical Abstract

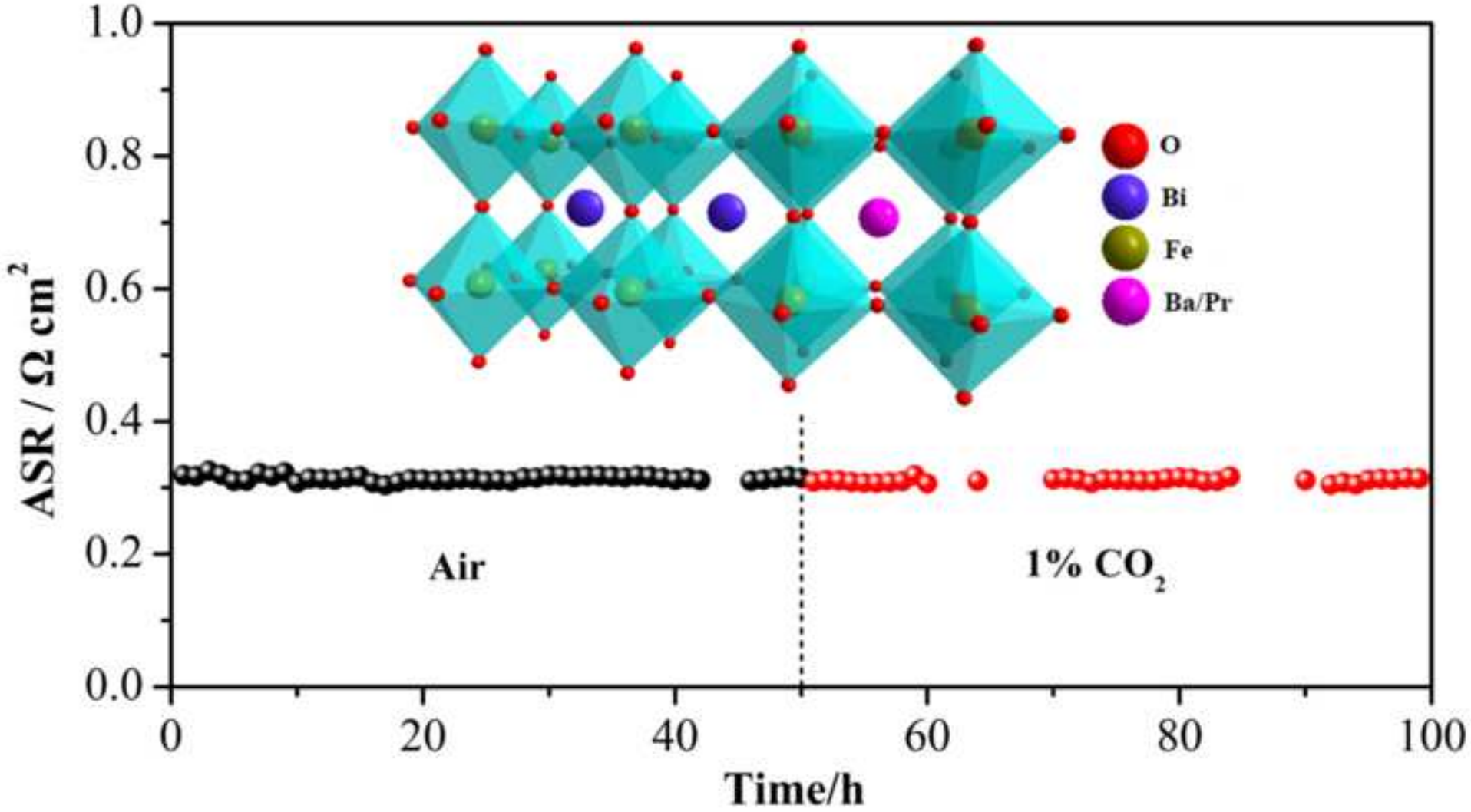

Highlights

- A novel perovskite cathode $Bi_{0.7}Pr_{0.1}Ba_{0.2}FeO_{3-\delta}$ (BPBF) was well developed.
- The composite BPBF-based cathode exhibits favorable ORR activity with low polarization ASR values.
- Excellent thermal/chemical stability is achieved in both pure air and 1 vol% CO_2-containing air.
- The intrinsic high acidity of Bi^{3+} and co-substitution of Ba/Pr enable stable high electrocatalytic activity.

An efficient and durable perovskite electrocatalyst for oxygen reduction in solid oxide fuel cells

Lu Li [a], Ziqi Kong [a], Bowen Yao [a], Hua Yang [a], Zhenghui Gao [a], Linji Xu [b], Feifei Dong [a,*], Meng Ni [c], Zhan Lin [a,*]

[a] *School of Chemical Engineering and Light Industry, Guangdong University of Technology, Guangzhou Higher Education Mega Center, Guangzhou 510006, P. R. China*

[b] *Environmental Engineering Technology Research Center, Chongqing Academy of Ecological and Environmental Sciences, Qishan Road 252, Yubei district, Chongqing 401147, P. R. China.*

[c] *Building Energy Research Group, Department of Building and Real Estate, The Hong Kong Polytechnic University, Hung Hom, Kowloon, Hong Kong 999077, P. R. China*

* **Corresponding authors.**

E-mail addresses: **dongff@gdut.edu.cn (F. Dong), zhanlin@gdut.edu.cn (Z. Lin).**

ABSTRACT

Achieving superior electrocatalytic activity and thermal/chemical stability of cathode materials is the key to high-performance and durable solid oxide fuel cells (SOFC). Here, we present a barium and praseodymium co-substituted perovskite $Bi_{0.7}Pr_{0.1}Ba_{0.2}FeO_{3-\delta}$ (BPBF), a cubic-symmetry oxide phase, as a candidate cathode material for SOFC, with a focus on its crystalline structure, oxygen transport, electrocatalytic activity, as well as structural and chemical stability. The BPBF-based cathode delivers superior electroactivity, with a polarization area-specific-resistance as low as 0.056 Ω cm^2 at 700 °C in symmetrical cells. Surprisingly, when exposed to both air and 1 vol% CO_2-containing air at 600 °C for 100 h, the electrode activity remains constant. The prominent thermal and chemical (CO_2 tolerance) stability can be ascribed to co-substitution of barium and praseodymium and high acidity of bismuth ions. Endowed with favorable electrocatalytic activity and excellent durability, the BPBF-based material can be a promising cathode to facilitate commercialization of SOFC technology.

***Keywords*:** Solid oxide fuel cells; Cathode; Oxygen reduction reaction; Perovskite; CO_2 tolerance

1. Introduction

Reducing the operating temperature of solid oxide fuel cells (SOFC) to facilitate their broad commercialization has been a global R&D trend [1-3]. For decades, tremendous efforts in SOFC field have been focused on the development of cathode materials, since the intrinsic temperature-dependence nature of oxygen reduction reaction (ORR) in cathode (i.e., the rate of ORR significantly decreases with decreasing temperatures) brings about a contradiction between reduced operating temperature and excellent cell performance [4,5]. As a kind of typical cathode materials, perovskite compounds with the general formula given as ABO_3, where A represents alkaline-earth or rare-earth metal cations and B is transition-metal cations, have drawn great attention benefited from their structural and compositional flexibility, high ORR activity, easy accessibility and environmental friendliness [1,6]. Recently, many iron-based perovskites, such as $La_{1-x}Sr_xFeO_{3-\delta}$ [7], $Ba_{1-x}La_xFeO_{3-\delta}$ [8], $BaNb_{0.05}Fe_{0.95}O_{3-\delta}$ [9], $BaFe_{0.95}Sn_{0.05}O_{3-\delta}$ [10], $Ba_{1-x}Sr_xZn_{1-y}Fe_yO_{3-\delta}$ [11], $Sr(Ti_{0.3}Fe_{0.7-x}Co_x)O_{3-\delta}$ [12], $SrSc_xTa_{0.1-x}Fe_{0.9}O_{3-\delta}$ [13], $PrBa(Fe_{0.8}Sc_{0.2})_2O_{5+\delta}$ [14], have been investigated as potential cathodes for SOFC due to the high mixed ionic and electronic conductivity as well as the relatively lower cost and thermal expansion coefficient in comparison with cobalt-based materials [15,16]. However, most of the iron-based perovskites developed so far still suffer from inferior electrocatalytic activity at reduced temperatures and poor structural and chemical stability against ambient atmosphere, hence considerably impeding their potential applications [17,18].

$BiFeO_3$, crystallizing a distorted rhombohedral structure with a R-3c space group

at room temperature, is a parent compound regarded as promising cathode candidates for SOFC [19-21]. Owing to the low basicity of Bi^{3+} and multiple oxidation states of Fe ions, $BiFeO_3$ can be expected to exhibit superior chemical stability under CO_2 exposure and desirable redox capability [22,23]. Furthermore, the high polarizability of Bi^{3+} induced by its 6s lone pair of electrons facilitates a high mobility of oxygen vacancies with a concurrent reduction of the vacancy migration enthalpy, which is crucial and beneficial for the electrocatalytic activity for ORR [16,22]. The major obstacles towards SOFC applications of $BiFeO_3$ derive from the redundant formation of impurity phases (such as $Bi_2Fe_4O_9$ and $Bi_{25}FeO_{40}$) during the synthesis process and the highly volatile nature of bismuth [24-26]. The former increases the difficulty and cost of material preparation and the later arouses the structural instability.

It has been reported that partial substitution of Bi site with other alkaline-earth or rare-earth metal cations (e.g., Sr^{2+}, Ba^{2+}, La^{3+}, $Pr^{3/4+}$, Cu^{2+}, Sb^{3+}, etc.) is a feasible avenue to overcome the aforementioned drawbacks [25,27-31]. For instance, Shisode et al. [32] successfully prepared single-phased $Bi_{1-x}Ba_xFeO_3$ using a cost-effective sol-gel method, the doping of Ba^{2+} substantially suppressed the secondary phase and promoted the formation of oxygen vacancies due to the lower valence of Ba^{2+} over Bi^{3+} (charge compensation). Also, Pr partial substitution for Bi was found to stabilize the crystal structure since the valence of Pr would change in response to the evaporation of Bi, thus maintaining the structural stability [31,33]. More recently, several attempts have been made to modulate the structural, magnetic, and ferroelectric properties of $BiFeO_3$ by co-doping Ba and Pr at Bi site [34,35]. It is noted that the co-substitution of

Ba and Pr could contribute to the improvement of structural symmetry, which is potentially beneficial to facilitate the migration of oxygen species in the transport process. However, few studies report the activity of catalyzing the ORR for Ba/Pr co-substituted $BiFeO_3$ perovskites as SOFC cathodes. Additionally, a decline of ORR activity could be observed with Pr co-substitution since the high-valence Pr ion substitution for Bi would hinder oxygen vacancy generation [33]. Incorporating electrolyte with a high ionic conductivity into cathode could be an effective strategy [36,37].

On the basis of the aforementioned progress, herein, we propose the development and characterization of a new perovskite cathode $Bi_{0.7}Pr_{0.1}Ba_{0.2}FeO_{3-\delta}$ (BPBF) for SOFC. To evaluate the potential application of composite BPBF-based cathode, the crystal structure, oxygen transport, electrochemical activity, structural and chemical stability are well investigated. Particularly, the stability testing on symmetrical cells in air prior and after introducing CO_2 shows an almost invariable outcome, suggesting a prominent CO_2 tolerance. Overall, a unique combination of low polarization resistance and high durability in air/CO_2 enables the new material a highly desirable oxygen reduction electrode for SOFC.

2. Experimental Section

2.1. Powder synthesis

$Bi_{0.7}Pr_{0.1}Ba_{0.2}FeO_{3-\delta}$ (BPBF) was prepared by a combined EDTA-citrate complexing sol-gel method. In brief, the stoichiometric amounts of metal nitrates,

weighed according to the desired nominal composition, were dissolved in deionized water to form a homogeneous solution. Notably, the required amount of dilute nitric acid was adopted to dissolve $Bi(NO_3)_3 \cdot 5H_2O$ to avoid its hydrolysis in water. The complexing agents (i.e., EDTA and citric acid (CA)), along with NH_3 aqueous solution (acting as pH regulator) were then added into the preceding solution in sequence with a molar ratio of total metal cations: EDTA: CA: $NH_3 \cdot H_2O$ = 1: 1: 2: 10. The resulting solution was dehydrated using a magnetic heated stirrer to yield a wet gel, which was then pretreated in an oven at 250 °C until a black solid precursor was formed. The precursor was subsequently calcined at 900 °C for 5 h in ambient air to attain the final powder with the intended perovskite structure.

2.2. Cell fabrication

Electrolyte ($Sm_{0.2}Ce_{0.8}O_{1.9}$, SDC)-supported symmetrical cells with the BPBF/SDC|SDC|BPBF/SDC configuration were adopted for evaluating the area specific resistances (ASR) of cathode. Typically, a dense 0.8 mm-thick SDC pellet with 12 mm-diameter was pressed using a stainless-steel die followed by sintering at 1350 °C for 5 h in air. The cathode ink, prepared by ball-milling (Fritsch, Pulverisette 6) the BPBF/SDC composite cathode at a weight ratio of 7:3 with a mixture of isopropanol, glycol, and glycerol, was spray-coated on both sides of a dense SDC electrolyte pellet. Subsequently, the symmetrical cells were sintered at 850 °C in ambient air for 2 h with a heating rate of 5 °C min^{-1}. Anode-supported single cells were fabricated by a co-pressing and co-sintering procedure and subjected to power output measurements. Firstly, the NiO-SDC anode powder mixture with a weight ratio of 6:4 was uniaxially

pressed into disk-like pellets and SDC electrolyte powder was sequentially deposited onto the disk surface, followed by co-sintering at 1400 °C for 5 h. The cathode ink was then sprayed on the electrolyte surface and calcined at 850 °C for 2 h. Silver paste was painted onto the electrode as current collector layer while silver wires served as leads for symmetrical and single cells.

2.3. Basic characterizations

The phase structure and purity of the as-synthesized samples were investigated by room-temperature X-ray diffraction (XRD, Rigaku MiniFlex600, Cu Kα radiation, λ = 1.54059 Å) operated at a tube voltage of 40 kV and a current of 40 mA. XRD patterns were refined using the Rietveld method by General Structure Analysis System (GSAS) software with the EXPGUI interface [38]. The microstructure and morphology of the powdered sample and tested cell were characterized using field-emission transmission electron microscope (FE-TEM, Talos F200S) equipped with an energy dispersive X-ray (EDX) spectrometer and field-emission scanning electron microscope (FE-SEM, Hitach, SU8220), respectively. The bar-shaped dense specimen with the geometric dimensions of ~ 2 mm × 5 mm × 12 mm was subjected to the electrical conductivity relaxation (ECR) assessments to obtain the chemical bulk diffusion coefficient (D_{chem}) and chemical surface exchange coefficient (k_{chem}). The detailed experimental procedure of ECR was reported in our previous work [39].

2.4. Electrochemical testing

The electrochemical impedance spectra (EIS) of the symmetrical cells were

acquired using a Solartron 1260 frequency response analyzer interfaced with a Solartron 1287 potentiostat. The data were collected with an AC amplitude of 10 mV in the frequency range from 100 kHz to 0.01 Hz in air or air containing 1% CO_2 concentration. The button cells were mounted on quartz supporting tube for fuel cell testing at 450-650 °C, with humidified hydrogen (3% H_2O) at a flow rate of 80 mL min^{-1} as the fuel and ambient air as the oxidant. The *I-V* polarization curves were monitored with a digital source meter (Keithley 2420).

3. Results and discussion

3.1. Phase structure

Shown in Fig. 1a is a schematic diagram of the crystal cell structure of Ba/Pr co-substituted $BiFeO_3$ specimen (BPBF) derived from XRD refinement (Fig. 1b). As expected, the sharp and characteristic peaks of well-crystallized BPBF could be ascribed to a single perovskite phase. The results on crystal structure extracted from Rietveld refinement exhibit a cubic symmetric structure of BPBF with $Pm\bar{3}m$ space group, illustrating that Ba/Pr doping at the A-site can repress the formation of impurities and facilitate a structural transformation from rhombohedral to cubic symmetry. The lattice parameters of BPBF converge to be 3.9691(4) Å (Table 1), which is in qualitative agreement with the previous study [34]. The reliability of the results is validated by the desirable refinement parameters with the weighted pattern R_{wp} = 6.59%, pattern R_p = 4.99%, and goodness of fit χ^2 = 0.9047, proving a good fit between the experimental data and calculated pattern. To evaluate the feasibility of the composite material, a 7:3

wt.% powder mixture of BPBF and SDC was fired at 900 °C for 5 h and afterwards subjected to XRD measurement (Fig. S1). No additional peaks emerge other than the original characteristic peaks assigned to BPBF and SDC phases, manifesting a good chemical compatibility between the constituents.

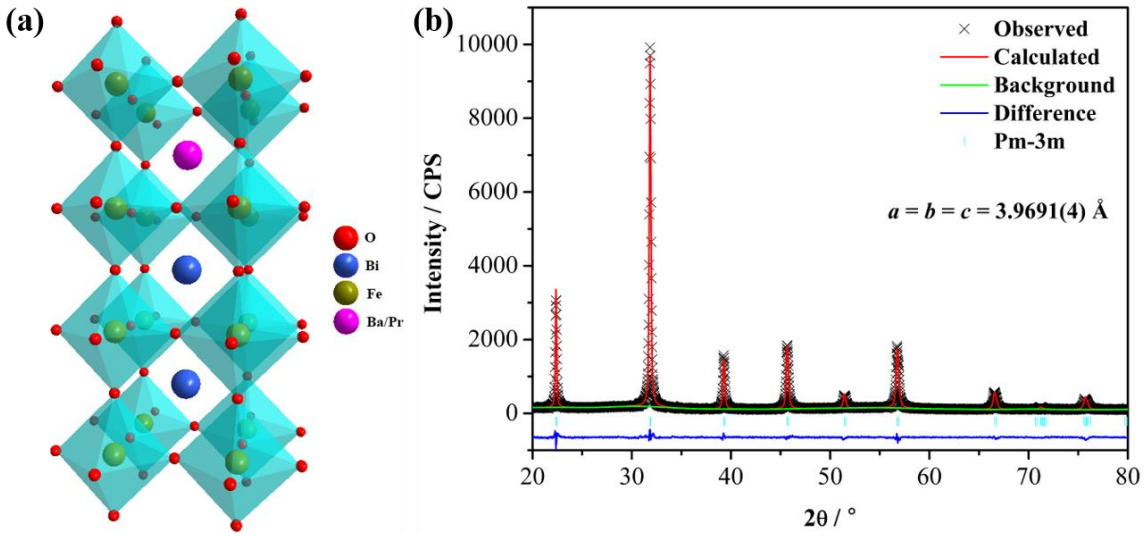

Fig. 1. (a) Schematic representation of the BPBF crystal structure. (b) Refined XRD profiles of the BPBF powdered sample.

Table 1. Crystallographic details of BPBF obtained from the Rietveld refinement of XRD data

Atom	*x*	*y*	*z*	Occupancy
Bi	0.0	0.0	0.0	0.7028
Pr	0.0	0.0	0.0	0.1061
Ba	0.0	0.0	0.0	0.1972
Fe	0.5	0.5	0.5	0.9911
O	0.5	0.5	0.0	0.9778

Space group: $Pm\bar{3}m$, $a = b = c = 3.9691(4)$ Å, $R_{wp} = 6.59\%$, $R_p = 4.99\%$, $\chi^2 = 0.9047$.

The phase and structural information in further detail were verified by high-resolution TEM (HR-TEM) images and their corresponding fast Fourier transform (FFT) patterns, recorded with the electron beam along the [$1\bar{1}0$] direction. Two magnified regions (Fig. 2b and c) selected from Fig. 2a both illustrate well-crystallized lattice fringes with similar interplanar spacing of ~0.279 and ~0.278 nm, as reflected in the respective intensity distribution patterns of lattice planes (Fig. 2d and e), matching well with the distance between the (110) crystal planes for a cubic perovskite structure. The observation of the distance of (001), (110), and (111) planes and the included angle (~ 55°) in the FFT patterns (Fig. 2f and g, corresponding to Fig. 2b and c, respectively) clearly confirms the cubic-symmetry perovskite structure of BPBF, consistent with the XRD analysis. According to the elemental distribution from EDX mapping characterization in Fig. S2, no segregation occurs due to the homogeneous distribution of Bi, Pr, Ba, and Fe elements in BPBF throughout the region.

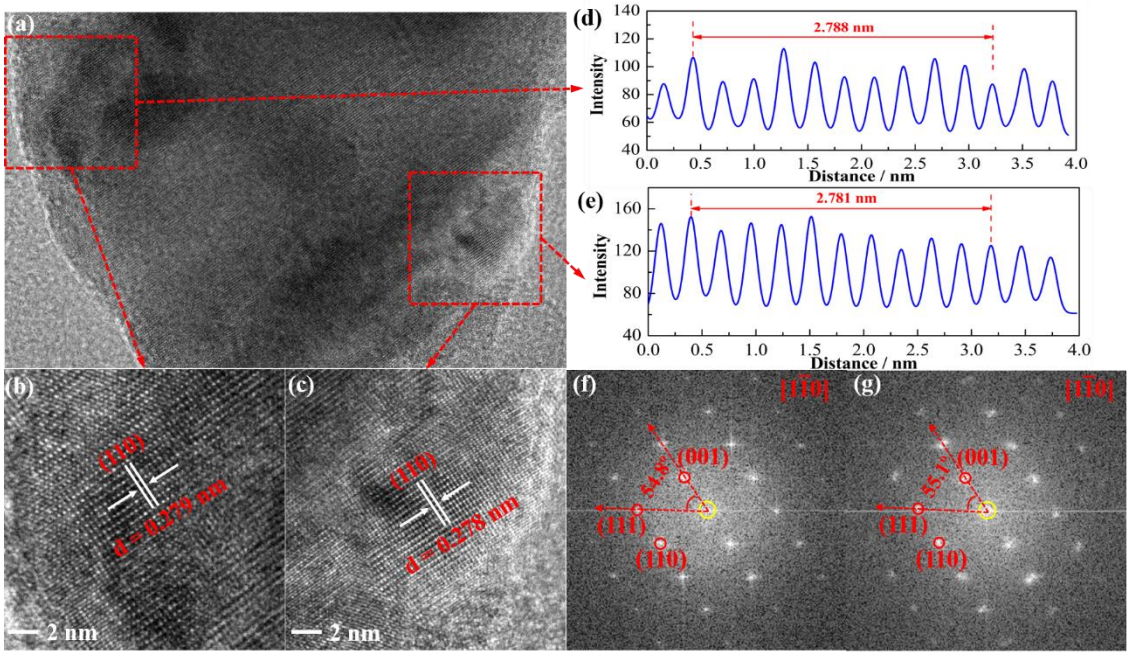

Fig. 2. Crystalline structure of BPBF. (a) HR-TEM image of the BPBF lattice. (b, c)

Emerging lattice fringes of two magnified view selected from (a). (d, e) Intensity distribution patterns of crystalline fringes corresponding to (b, c), respectively. (f, g) Corresponding FFT patterns from (b, c) respectively along [$1\bar{1}0$] zone axis.

3.2. Oxygen transport

Superior kinetics of ORR (i.e., the rates of bulk diffusion and surface exchange for oxygen) is a necessary and intrinsic condition for favorable electrocatalytic performance. Shown in Fig. 3a are typical relaxation curves for electrical conductivity when abruptly transforming the oxygen partial pressure from 0.10 to 0.21 atm under different temperatures. The fast approach of electrical conductivity to a new equilibrium is observed, indicating promising oxygen transport properties. The values of D_{chem} and k_{chem} obtained by fitting the relaxation curves using Fick's second law under appropriate initial and boundary conditions are plotted in Arrhenius form in Fig. 3b. It is clear that both D_{chem} and k_{chem} rise as temperature increases due to the thermally activated migration process. BPBF achieves a desirable oxygen catalytic activity, e.g., D_{chem} = 4.43×10^{-4} cm^2 s^{-1} and k_{chem} = 4.70×10^{-3} cm s^{-1} at 600 °C, which is comparable to that of the prevailing perovskite oxides [40,41]. The fast oxygen kinetics could be attributed to the reduced vacancy migration enthalpy resulting from the high content of Bi and the cubic structure with enhanced symmetry caused by the co-substitution of Ba and Pr.

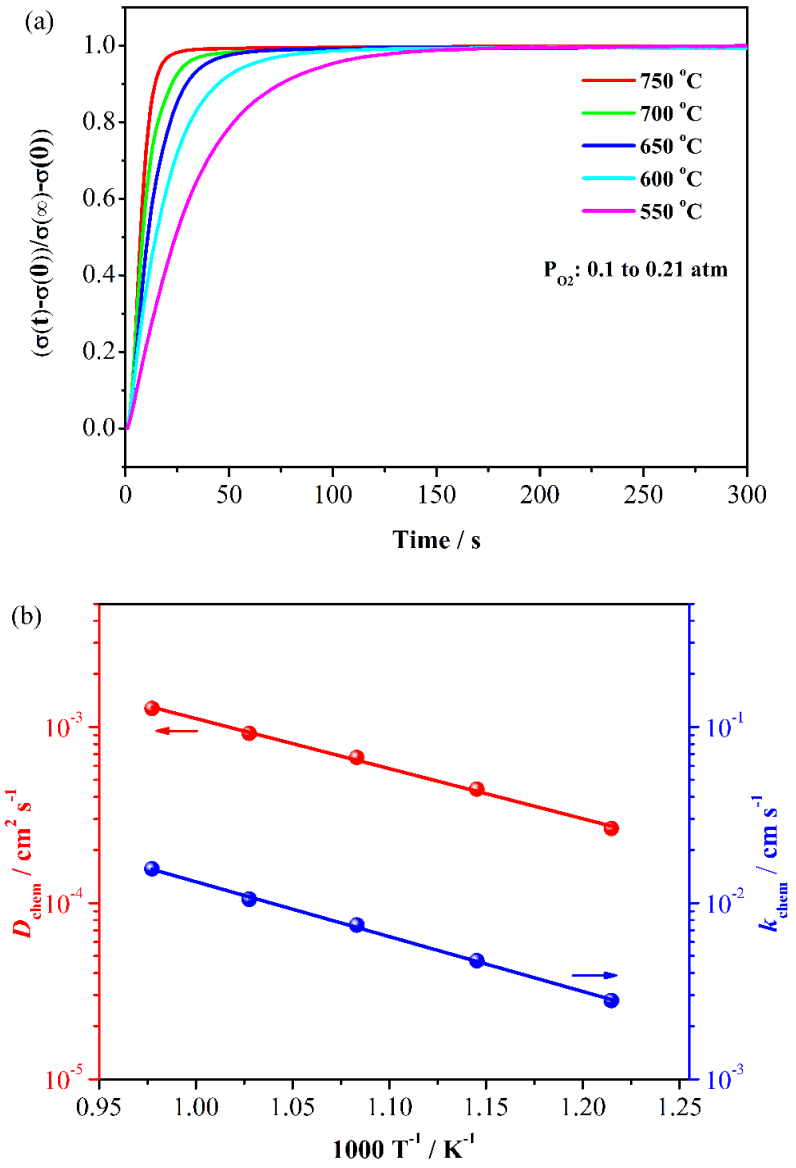

Fig. 3. (a) ECR response curves of BPBF at various temperatures after an abrupt change in the oxygen partial pressure from 0.1 to 0.21 atm. (b) Temperature dependence of the fitted D_{chem} and k_{chem}.

3.3. Electrocatalytic activity

To assess the electrocatalytic activity toward oxygen reduction, the EIS measurements were performed on symmetrical cells with a configuration of BPBF/SDC|SDC|BPBF/SDC. Fig. 4a shows the typical Nyquist plots of EIS data

acquired at 550-750 °C under open circuit condition. The electrode polarization ASR can be extracted from the difference between the intercepts of impedance loop on the real axis at high and low frequencies, as also exhibited in an Arrhenius plot in Fig. 4b. The electrode exhibits favorable ORR activity at intermediate-temperature range as embodied by the low ASR values (e.g., 0.056 Ω cm^2 at 700 °C). The electrochemical activity of the cathode reported here (Fig. 4b) is comparable to that of the iron-based benchmark perovskite cathodes [42-46]. Moreover, the cathode exhibits a relatively low activation energy of 1.25 eV, signifying a lower energy barrier for ORR. Additionally, single cells with BPBF-based oxygen electrode, conventional SDC thin-film electrolyte (20 μm), and Ni-SDC fuel electrode yield acceptable electrochemical performance at intermediate temperatures, e.g., 546 mW cm^{-2} at 600 °C (Fig. S3), which is superior to that of the conventional cathode materials (such as Sr-doped $LaMnO_3$, $La_{0.6}Sr_{0.4}Co_{0.2}Fe_{0.8}O_{3-\delta}$) [47, 48]. As seen from the cross-sectional view of the tested cell in Fig. S4, the BPBF-based cathode remains well-porous structure and firmly adheres to the electrolyte without crack or delamination. More competitive performance is expected to be effectively achieved by applying the state-of-the-art thin-film technology and microstructural optimization for electrolyte and fuel-electrode processing, respectively.

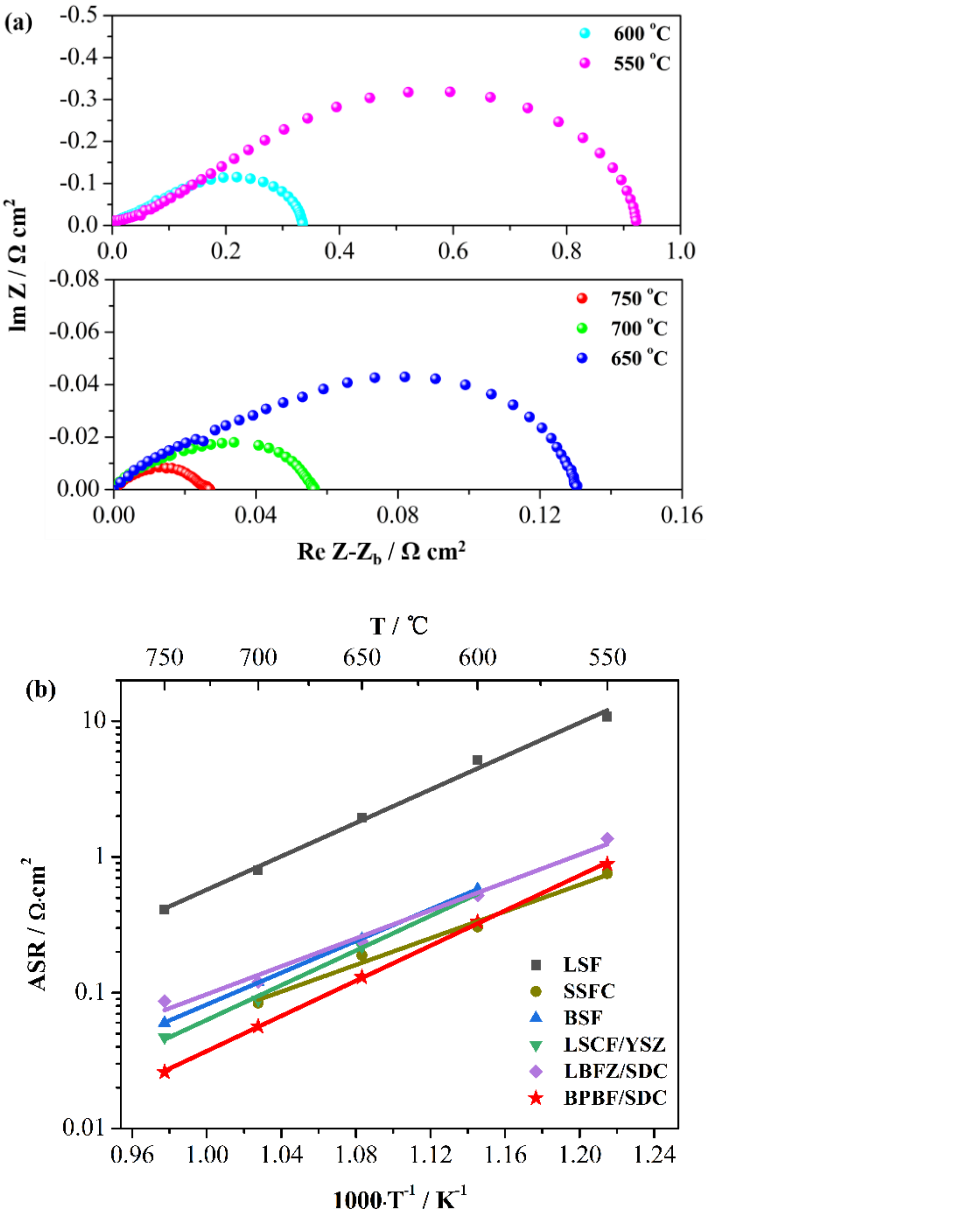

Fig. 4. (a) Nyquist plots of the impedance spectra of BPBF-based symmetrical cells. The ohmic resistances from the electrolyte are subtracted for direct comparison. (b) Performance mapping of the derived polarization ASR values of the BPBF-based cathode against other iron-based benchmark perovskite cathodes, such as $La_{0.5}Sr_{0.5}FeO_{3-\delta}$ (LSF) [42], $Sm_{0.5}Sr_{0.5}Fe_{0.8}Cu_{0.2}O_{3-\delta}$ (SSFC) [43], $Bi_{0.5}Sr_{0.5}FeO_{3-\delta}$ (BSF) [44], $La_{0.8}Sr_{0.2}Co_{0.5}Fe_{0.5}O_{3-\delta}$/YSZ (LSCF/YSZ) [45], $La_{0.4}Ba_{0.6}Fe_{0.8}Zn_{0.2}O_{3-\delta}$/SDC (LBFZ/SDC) [46].

3.4. Durability in air with CO_2

Apart from superior electrocatalytic activity for ORR, excellent durability of cathode is also significant to substantiate its practical application in SOFC, especially when exposed to contaminants (e.g., CO_2) -containing atmosphere [49]. The long-term stability was monitored by determining the ASR values of the cathode using symmetrical button cells aged at 600 °C in air prior and after introducing 1 vol% concentration of CO_2 into the air atmosphere over respective 50 h-testing duration, as displayed in Fig. 5. The insets are the corresponding Nyquist plots of electrode at the initial and terminal time in different atmospheres. Clearly, the polarization ASR values remain almost constant at about 0.31 Ω cm^2 during the first 50 h operation in pure air, which can also be validated by the primarily overlapped impedance spectra over the 50 h duration. When introducing CO_2 into the air stream, surprisingly, ASR remains stable and unchanged during another 50 h run, as evidenced by the invariable evolution of impedance loop in the inset. The results above suggest the exceptional durability and CO_2 tolerance of the BPBF/SDC electrode, which outperform other state-of-the-art cathode materials [50-52]. The co-substitution of Ba/Pr and high acidity of Bi^{3+} could contribute to the outstanding durability and CO_2 tolerance of BPBF-based cathode, highlighting the practical application towards commercialization of SOFC.

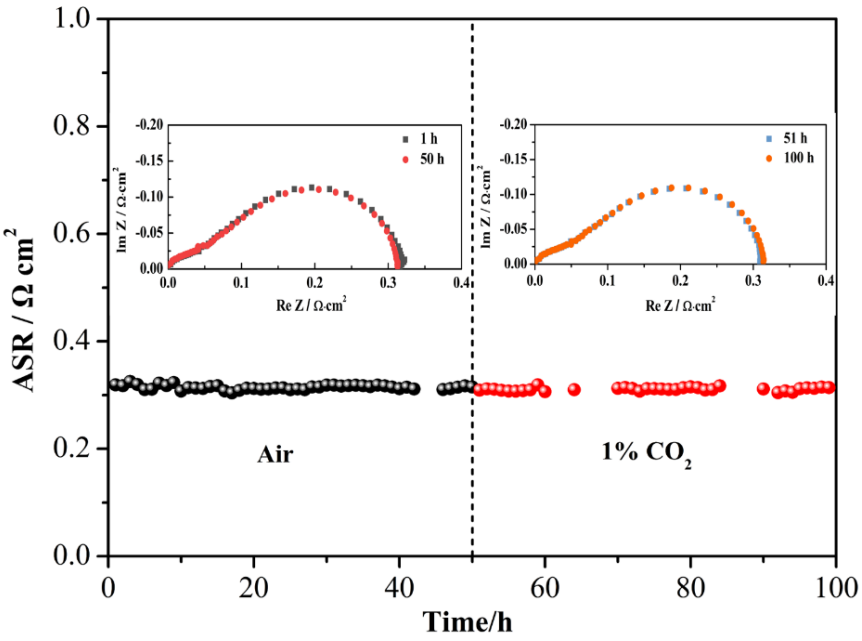

Fig. 5. Durability of polarization ASR values at 600 °C in air and 1 vol% CO_2, respectively. Insets are the corresponding Nyquist plots in different atmospheres.

It is well known that state-of-the-art $Ba_{0.5}Sr_{0.5}Co_{0.8}Fe_{0.2}O_{3-\delta}$ (BSCF) suffers from performance degradation during SOFC operation due to its instability, thus eliminating it from practical application [53]. It follows that maintaining the excellent durability requires both thermal and chemical stability of the cathode materials. Accordingly, the complementary characterizations (e.g., XRD and TEM) are performed to cross-check the operational durability regarding thermal and chemical stability. As shown in Fig. S5, after exposure to both pure air and 1 vol% CO_2-containing air at 600 °C for 100 h, no pronounced change and no emergence of any secondary phase (such as carbonate species) are observed from the XRD patterns of as-prepared BPBF. Furthermore, the Rietveld refinement based on the XRD patterns reveals the preserved cubic-symmetry structure, and the obtained structural information listed in Tables S1 and S2 is analogous to that of the fresh specimen. These results clearly demonstrate the thermal

and chemical stability of the electrode material, namely the remarkable endurance in air and CO_2-containing air. Simultaneously, the crystallized lattice planes of HR-TEM images (Fig. S6) taken after the same long-term treatment as XRD characterization show no significant change in comparison with those of the original sample, confirming the robust reliability against air (CO_2), consistent with the XRD analysis. In addition, evaluation of compatibility with SDC annealed in both pure air and air containing 1 vol% CO_2 at 600 °C for 100 h was performed, as plotted in Fig. S7. The respective phase structures of the BPBF and SDC are retained in both cases, since no extra diffraction peaks are detected, indicating almost no chemical reaction between them. The aforementioned consequence is in accordance with the electrochemical assessment of the BPBF electrode material discussed earlier.

4. Conclusion

To summarize, a new perovskite oxide phase $Bi_{0.7}Pr_{0.1}Ba_{0.2}FeO_{3-\delta}$ (BPBF), with superior electrocatalytic activity and durability, has been fabricated and evaluated as a cathode material for SOFC. Benefited from cubic-symmetry phase structure and fast kinetics of oxygen transport, the BPBF-based cathode exhibits favorable ORR activity with a low ASR value of 0.056 Ω cm^2 at 700 °C. More surprisingly, the cathode also displays excellent thermal and chemical stability against CO_2, validated by the steady and unchanged ASR values in air prior and after introducing 1 vol% CO_2 over 100 h duration. The intrinsic high acidity of Bi^{3+} and co-substitution of Ba/Pr enable stable high electrocatalytic activity. These results underline the strong potential of the BPBF-based materials in devices involving oxygen electrochemistry, such as solid oxide

fuel/electrolysis cells, oxygen separation membranes, oxygen pumps, and oxygen sensors.

Declaration of competing interest

The authors declare that they have no known competing financial interests or personal relationships that could have appeared to influence the work reported in this paper.

Acknowledgements

This work was financially supported by a startup R&D funding from One-Hundred Young Talents Program of Guangdong University of Technology (No.: 220413180), a Foundation for Youth Innovative Talents in Higher Education of Guangdong Province (No.: 2018KQNCX060), Joint Funds of Basic and Applied Basic Research Foundation of Guangdong Province (No. 2019A1515110322), a grant from Research Grant Council, University Grants Committee, Hong Kong SAR (No.: PolyU 152064/18E), a funding from Research Incentive Performance Program of Chongqing Science and Technology Bureau (cstc2018jszx-zdyfxmX0016).

Appendix A. Supplementary data

Supplementary material related to this article can be found, in the online version, at

Nomenclature and abbreviations

SOFC	solid oxide fuel cell
ORR	oxygen reduction reaction

CA	citric acid
ASR	area specific resistance
ECR	electrical conductivity relaxation
D_{chem}	chemical bulk diffusion coefficient
k_{chem}	chemical surface exchange coefficient
EIS	electrochemical impedance spectra
XRD	X-ray diffraction
GSAS	General Structure Analysis System
FE-TEM	field-emission transmission electron microscope
EDX	energy dispersive X-ray
FE-SEM	field-emission scanning electron microscope
HR-TEM	high-resolution transmission electron microscope
FFT	fast Fourier transform
BPBF	$Bi_{0.7}Pr_{0.1}Ba_{0.2}FeO_{3-\delta}$
SDC	$Sm_{0.2}Ce_{0.8}O_{1.9}$
LSF	$La_{0.5}Sr_{0.5}FeO_{3-\delta}$
SSFC	$Sm_{0.5}Sr_{0.5}Fe_{0.8}Cu_{0.2}O_{3-\delta}$
BSF	$Bi_{0.5}Sr_{0.5}FeO_{3-\delta}$
LSCF/YSZ	$La_{0.8}Sr_{0.2}Co_{0.5}Fe_{0.5}O_{3-\delta}/Y_{0.16}Zr_{0.92}O_{2.08}$
LBFZ/SDC	$La_{0.4}Ba_{0.6}Fe_{0.8}Zn_{0.2}O_{3-\delta}/Sm_{0.2}Ce_{0.8}O_{1.9}$
BSCF	$Ba_{0.5}Sr_{0.5}Co_{0.8}Fe_{0.2}O_{3-\delta}$

References

[1] E.D. Wachsman, K.T. Lee, Lowering the temperature of solid oxide fuel cells, Science 334 (2011) 935–939. https://doi.org/10.1126/science.1204090.

[2] Y. Xie, H. Ding, X. Xue, Direct methane fueled solid oxide fuel cell model with detailed reforming reactions, Chem. Eng. J. 228 (2013) 917–924. https://doi.org/10.1016/j.cej.2013.05.084.

[3] H. Zhang, W. Kong, F. Dong, H. Xu, B. Chen, M. Ni, Application of cascading thermoelectric generator and cooler for waste heat recovery from solid oxide fuel cells, Energy Convers. Manag. 148 (2017) 1382–1390. https://doi.org/10.1016/j.enconman.2017.06.089.

[4] S.B. Adler, Factors governing oxygen reduction in solid oxide fuel cell cathodes, Chem. Rev. 104 (2004) 4791–4843. https://doi.org/10.1021/cr020724o.

[5] A.J. Jacobson, Materials for solid oxide fuel cells, Chem. Mater. 22 (2010) 660–674. https://doi.org/10.1021/cm902640j.

[6] Y. Gao, D. Chen, M. Saccoccio, Z. Lu, F. Ciucci, From material design to mechanism study: Nanoscale Ni exsolution on a highly active A-site deficient anode material for solid oxide fuel cells, Nano Energy 27 (2016) 499–508. https://10.1016/j.nanoen.2016.07.013.

[7] Y. Huang, J.M. Vohs, R.J. Gorte, Fabrication of Sr-doped $LaFeO_3$ YSZ composite cathodes, J. Electrochem. Soc. 151 (2004) 646–651. https://doi.org/10.1149/1.1652053.

[8] F. Dong, D. Chen, Y. Chen, Q. Zhao, Z. Shao, La-doped $BaFeO_{3-\delta}$ perovskite as a cobalt-free oxygen reduction electrode for solid oxide fuel cells with oxygen-ion conducting electrolyte, J. Mater. Chem. 22 (2012) 15071–15079. https://doi.org/10.1039/c2jm31711g.

[9] F. Dong, Y. Chen, R. Ran, D. Chen, M.O. Tadé, S. Liu, Z. Shao, $BaNb_{0.05}Fe_{0.95}O_{3-\delta}$ as a new oxygen reduction electrocatalyst for intermediate temperature solid oxide fuel cells, J. Mater. Chem. A 1 (2013) 9781–9791. https://doi.org/10.1039/c3ta11447c.

[10] F. Dong, M. Ni, W. He, Y. Chen, G. Yang, D. Chen, Z. Shao, An efficient electrocatalyst as cathode material for solid oxide fuel cells: $BaFe_{0.95}Sn_{0.05}O_{3-\delta}$, J. Power Sources 326 (2016) 459–465. https://doi.org/10.1016/j.jpowsour.2016.07.023.

[11] B. Wei, Z. Lü, X. Huang, M. Liu, N. Li, W. Su, Synthesis, electrical and electrochemical properties of $Ba_{0.5}Sr_{0.5}Zn_{0.2}Fe_{0.8}O_{3-\delta}$ perovskite oxide for IT-SOFC cathode, J. Power Sources 176 (2008) 1–8. https://doi.org/10.1016/j.jpowsour.2007.09.120.

[12] S.L. Zhang, H. Wang, M.Y. Lu, A.P. Zhang, L. V. Mogni, Q. Liu, C.X. Li, C.J. Li, S.A. Barnett, Cobalt-substituted $SrTi_{0.3}Fe_{0.7}O_{3-\delta}$: a stable high-performance oxygen electrode material for intermediate-temperature solid oxide electrochemical cells, Energy Environ. Sci. 11 (2018) 1870–1879. https://doi.org/10.1039/c8ee00449h.

[13] Y. Zhang, X. Gao, J. Sunarso, B. Liu, W. Zhou, M. Ni, Z. Shao, Significantly improving the durability of single-chamber solid oxide fuel cells: a highly active CO_2-resistant perovskite cathode, ACS Appl. Energy Mater. 1 (2018) 1337–1343. https://doi.org/10.1021/acsaem.8b00051.

[14] W. He, X. Wu, F. Dong, M. Ni, A novel layered perovskite electrode for symmetrical solid oxide fuel cells: $PrBa(Fe_{0.8}Sc_{0.2})_2O_{5+\delta}$, J. Power Sources 363 (2017) 16–19. https://doi.org/10.1016/j.jpowsour.2017.07.059.

[15] A. Mai, V.A.C. Haanappel, F. Tietz, D. Stöver, Ferrite-based perovskites as cathode materials for anode-supported solid oxide fuel cells. Part II. Influence of the CGO interlayer, Solid State Ion. 177 (2006) 2103–2107. https://doi.org/10.1016/j.ssi.2005.12.010.

[16] X. Song, S. Le, X. Zhu, L. Qin, Y. Luo, Y. Li, K. Sun, Y. Chen, High performance $BaFe_{1-x}Bi_xO_{3-\delta}$ as cobalt-free cathodes for intermediate temperature solid oxide fuel cells, Int. J. Hydrogen Energy 42 (2017) 15808–15817. https://doi.org/10.1016/j.ijhydene.2017.05.061.

[17] X. Yu, W. Long, F. Jin, T. He, Cobalt-free perovskite cathode materials $SrFe_{1-x}Ti_xO_{3-\delta}$ and performance optimization for intermediate-temperature solid oxide fuel cells, Electrochim. Acta 123 (2014) 426–434. https://doi.org/10.1016/j.electacta.2014.01.020.

[18] E.V. Tsipis, V.V. Kharton, Electrode materials and reaction mechanisms in solid oxide fuel cells: a brief review. III. Recent trends and selected methodological aspects, J. Solid State Electrochem. 15 (2011) 1007–1040. https://doi.org/10.1007/s10008-011-1341-8.

[19] S. Thakur, O.P. Pandey, K. Singh, Structural, thermal and electrical study of Ca^{2+}, Sr^{2+} substituted $BiFeO_3$ for IT-SOFC, ECS Trans. 57 (2013) 2125–2132.

https://doi.org/10.1149/05701.2125ecst.

[20] E. Heifets, E.A. Kotomin, A.A. Bagaturyants, J. Maier, Ab initio study of $BiFeO_3$: thermodynamic stability conditions, J. Phys. Chem. Lett. 6 (2015) 2847–2851. https://doi.org/10.1021/acs.jpclett.5b01071.

[21] R.A. Afzal, K.Y. Park, S.H. Cho, N.I. Kim, S.R. Choi, J.H. Kim, H.T. Lim, J.Y. Park, Oxygen electrode reactions of doped $BiFeO_3$ materials for low and elevated temperature fuel cell applications, RSC Adv. 7 (2017) 47643–47653. https://doi.org/10.1039/c7ra08671g.

[22] A. Wedig, R. Merkle, B. Stuhlhofer, H.U. Habermeier, J. Maier, E. Heifets, Fast oxygen exchange kinetics of pore-free $Bi_{1-x}Sr_xFeO_{3-\delta}$ thin films, Phys. Chem. Chem. Phys. 13 (2011) 16530–16533. https://doi.org/10.1039/c1cp21684h.

[23] A.J. Fernández-Ropero, J.M. Porras-Vázquez, A. Cabeza, P.R. Slater, D. Marrero-López, E.R. Losilla, High valence transition metal doped strontium ferrites for electrode materials in symmetrical SOFCs, J. Power Sources 249 (2014) 405–413. https://doi.org/10.1016/j.jpowsour.2013.10.118.

[24] X. Wen, Z. Chen, E. Liu, X. Lin, C. Chen, Effect of Ba and Mn doping on microstructure and multiferroic properties of $BiFeO_3$ ceramics, J. Alloys Compd. 678 (2016) 511–517. https://doi.org/10.1016/j.jallcom.2016.04.029.

[25] E. Mostafavi, A. Ataie, M. Ahmadzadeh, M. Palizdar, T.P. Comyn, A.J. Bell, Synthesis of nano-structured $Bi_{1-x}Ba_xFeO_3$ ceramics with enhanced magnetic and electrical properties, Mater. Chem. Phys. 162 (2015) 106–112. https://doi.org/10.1016/j.matchemphys.2015.05.017.

[26] T. Soltani, B.K. Lee, Novel and facile synthesis of Ba-doped $BiFeO_3$ nanoparticles and enhancement of their magnetic and photocatalytic activities for complete degradation of benzene in aqueous solution, J. Hazard. Mater. 316 (2016) 122–133. https://doi.org/10.1016/j.jhazmat.2016.03.052.

[27] L. Gao, M. Zhu, Q. Li, L. Sun, H. Zhao, J.C. Grenier, Electrode properties of Cu-doped $Bi_{0.5}Sr_{0.5}FeO_{3-\delta}$ cobalt-free perovskite as cathode for intermediate-temperature solid oxide fuel cells, J. Alloys Compd. 700 (2017) 29–36. https://doi.org/10.1016/j.jallcom.2017.01.026.

[28] M. Li, Y. Ren, Z. Zhu, S. Zhu, F. Chen, Y. Zhang, C. Xia, $La_{0.4}Bi_{0.4}Sr_{0.2}FeO_{3-\delta}$ as cobalt-free cathode for intermediate-temperature solid oxide fuel cell, Electrochim. Acta 191 (2016) 651–660. https://doi.org/10.1016/j.electacta.2016.01.164.

[29] M. Li, Y. Wang, Y. Wang, F. Chen, C. Xia, Bismuth doped lanthanum ferrite perovskites as novel cathodes for intermediate-temperature solid oxide fuel cells, ACS Appl. Mater. Interfaces 6 (2014) 11286–11294. https://doi.org/10.1021/am5017045.

[30] L. Gao, Q. Li, L. Sun, T. Xia, L. Huo, H. Zhao, J.C. Grenier, Antimony-doped $Bi_{0.5}Sr_{0.5}FeO_{3-\delta}$ as a novel Fe-based oxygen reduction electrocatalyst for solid oxide fuel cells below 600 °C, J. Mater. Chem. A 6 (2018) 15221–15229. https://doi.org/10.1039/c8ta04222e.

[31] B. Yu, M. Li, Z. Hu, L. Pei, D. Guo, X. Zhao, S. Dong, Enhanced multiferroic properties of the high-valence Pr doped $BiFeO_3$ thin film, Appl. Phys. Lett. 93 (2008) 182909. https://doi.org/10.1063/1.3020296.

[32] M. V. Shisode, D.N. Bhoyar, P.P. Khirade, K.M. Jadhav, Structural, microstructural, magnetic, and ferroelectric properties of Ba^{2+}-doped $BiFeO_3$ nanocrystalline multifferroic material, J. Supercond. Novel Magn. 31 (2018) 2501–2509. https://doi.org/10.1007/s10948-017-4515-5.

[33] I. Coondoo, N. Panwar, I. Bdikin, V.S. Puli, R.S. Katiyar, A.L. Kholkin, Structural,

morphological and piezoresponse studies of Pr and Sc co-substituted $BiFeO_3$ ceramics, J. Phys. D: Appl. Phys. 45 (2012) 055302. https://doi.org/10.1088/0022-3727/45/5/055302.

[34] G.F. Cheng, Y.J. Ruan, W. Liu, X.S. Wu, Effect of temperature on structural expansion for $Bi_{0.8-x}Pr_xBa_{0.2}FeO_3$ ($x \leq 0.1$) ceramics, Thermochim. Acta 602 (2015) 74–77. https://doi.org/10.1016/j.tca.2015.01.011.

[35] G.F. Cheng, Y.H. Huang, J.J. Ge, B. Lv, X.S. Wu, Effects of local structural distortion on magnetization in $BiFeO_3$ with Pr, Ba co-doping, J. Appl. Phys. 111 (2012) 07C707. https://doi.org/10.1063/1.3673821.

[36] M. Balaguer, V.B. Vert, L. Navarrete, J.M. Serra, SOFC composite cathodes based on LSM and co-doped cerias ($Ce_{0.8}Gd_{0.1}X_{0.1}O_{2-\delta}$, X = Gd, Cr, Mg, Bi, Ce), J. Power Sources 223 (2013) 214–220. https://doi.org/10.1016/j.jpowsour.2012.09.060.

[37] J. Kim, W. Seo, J. Shin, M. Liu, G. Kim, Composite cathodes composed of $NdBa_{0.5}Sr_{0.5}Co_2O_{5+\delta}$ and $Ce_{0.9}Gd_{0.1}O_{1.95}$ for intermediate-temperature solid oxide fuel cells, J. Mater. Chem. A 1 (2013) 515–519. https://doi.org/10.1039/c2ta00025c.

[38] B.H. Toby, EXPGUI, a graphical user interface for GSAS, J. Appl. Crystallogr. 34 (2001) 210–213. https://doi.org/10.1107/S0021889801002242.

[39] L. Li, H. Yang, Z. Gao, Y. Zhang, F. Dong, G. Yang, M. Ni, Z. Lin, Nickel-substituted $Ba_{0.5}Sr_{0.5}Co_{0.8}Fe_{0.2}O_{3-\delta}$: a highly active perovskite oxygen electrode for reduced-temperature solid oxide fuel cells, J. Mater. Chem. A 7 (2019) 12343–12349. https://doi.org/10.1039/c9ta02548k.

[40] B. Qian, Y. Chen, M.O. Tade, Z. Shao, $BaCo_{0.6}Fe_{0.3}Sn_{0.1}O_{3-\delta}$ perovskite as a new superior oxygen reduction electrode for intermediate-to-low temperature solid oxide fuel cells, J. Mater. Chem. A 2 (2014) 15078–15086. https://doi.org/10.1039/c4ta02869d.

[41] Y. Chen, B. Qian, Z. Shao, Tin and iron co-doping strategy for developing active and stable oxygen reduction catalysts from $SrCoO_{3-\delta}$ for operating below 800 °C, J. Power Sources 294 (2015) 339–346. https://doi.org/10.1016/j.jpowsour.2015.06.095.

[42] Y. Niu, J. Sunarso, F. Liang, W. Zhou, Z. Zhu, Z. Shao, A comparative study of oxygen reduction reaction on Bi-and La-doped $SrFeO_{3-\delta}$ perovskite cathodes, J. Electrochem. Soc. 158 (2011) 132–138. https://doi.org/10.1149/1.3521316.

[43] Y. Ling, L. Zhao, B. Lin, Y. Dong, X. Zhang, G. Meng, X. Liu, Investigation of cobalt-free cathode material $Sm_{0.5}Sr_{0.5}Fe_{0.8}Cu_{0.2}O_{3-\delta}$ for intermediate temperature solid oxide fuel cell, Int. J. Hydrogen Energy 35 (2010) 6905–6910. https://doi.org/10.1016/j.ijhydene.2010.04.021.

[44] Y. Niu, W. Zhou, J. Sunarso, L. Ge, Z. Zhu, Z. Shao, High performance cobalt-free perovskite cathode for intermediate temperature solid oxide fuel cells, J. Mater. Chem. 20 (2010) 9619–9622. https://doi.org/10.1039/c0jm02816a.

[45] J. Chen, F. Liang, L. Liu, S. Jiang, B. Chi, J. Pu, J. Li, Nano-structured (La, Sr)(Co, Fe)O_3 + YSZ composite cathodes for intermediate temperature solid oxide fuel cells, J. Power Sources 183 (2008) 586–589. https://doi.org/10.1016/j.jpowsour.2008.05.082.

[46] Y.F. Bu, D. Ding, S.Y. Lai, D.C. Chen, X.H. Xiong, T. Wei, Q. Zhong, Evaluation of $La_{0.4}Ba_{0.6}Fe_{0.8}Zn_{0.2}O_{3-\delta}$ + $Sm_{0.2}Ce_{0.8}O_{1.9}$ as a potential cobalt-free composite cathode for intermediate temperature solid oxide fuel cells, J. Power Sources 275 (2015) 808–814. https://doi.org/10.1016/j.jpowsour.2014.11.085.

[47] F. Liang, J. Chen, S.P. Jiang, B. Chi, J. Pu, J. Li, High performance solid oxide fuel cells with

electrocatalytically enhanced (La, Sr)MnO_3 cathodes, Electrochem. Commun. 11 (2009) 1048–1051. https://doi.org/10.1016/j.elecom.2009.03.009.

[48] Z. Liu, M. Liu, L. Yang, M. Liu, LSM-infiltrated LSCF cathodes for solid oxide fuel cells, J. Energy Chem. 22 (2013) 555–559. https://doi.org/10.1016/S2095-4956(13)60072-8.

[49] C. Duan, D. Hook, Y. Chen, J. Tong, R. O'Hayre, Zr and Y co-doped perovskite as a stable, high performance cathode for solid oxide fuel cells operating below 500 °C, Energy Environ. Sci. 10 (2017) 176–182. https://doi.org/10.1039/c6ee01915c.

[50] Z. Zhang, D. Chen, J. Wang, S. Tan, X. Yu, Z. Shao, Highly active and stable cobalt-free hafnium-doped $SrFe_{0.9}Hf_{0.1}O_{3-\delta}$ perovskite cathode for solid oxide fuel cells, ACS Appl. Energy Mater. 1 (2018) 2134–2142. https://doi.org/10.1021/acsaem.8b00198.

[51] J. Wang, Z. Yang, Y. Lv, F. Jiang, Y. Chen, S. Peng, Effect of CO_2 on $La_{0.4}Sr_{0.6}Co_{0.2}Fe_{0.7}Nb_{0.1}O_{3-\delta}$ cathode for solid oxide fuel cells, J. Electroanal. Chem. 847 (2019) 113256. https://doi.org/10.1016/j.jelechem.2019.113256.

[52] Y. Meng, L. Sun, J. Gao, W. Tan, C. Chen, J. Yi, H.J.M. Bouwmeester, Z. Sun, K.S. Brinkman, Insights into the CO_2 stability-performance trade-off of antimony-doped $SrFeO_{3-\delta}$ perovskite cathode for solid oxide fuel cells, ACS Appl. Mater. Interfaces 11 (2019) 11498–11506. https://doi.org/10.1021/acsami.9b00876.

[53] A. Yan, M. Cheng, Y. Dong, W. Yang, V. Maragou, S. Song, P. Tsiakaras, Investigation of a $Ba_{0.5}Sr_{0.5}Co_{0.8}Fe_{0.2}O_{3-\delta}$ based cathode IT-SOFC. I. The effect of CO_2 on the cell performance, Appl. Catal. B Environ. 66 (2006) 64–71. https://doi.org/10.1016/j.apcatb.2006.02.021.